crystals

MDPI

Article

# Genesis of Complex Polyiodide Networks: Insights on the Blue Box/$I^-$/$I_2$ Ternary System

**Matteo Savastano *, Carla Bazzicalupi *, Cristina Gellini and Antonio Bianchi**

Department of Chemistry "Ugo Schiff", University of Florence, Via della Lastruccia, 3-13, 50019 Sesto Fiorentino, Italy; cristina.gellini@unifi.it (C.G.); antonio.bianchi@unifi.it (A.B.)

* Correspondence: matteo.savastano@unifi.it (M.S.); carla.bazzicalupi@unifi.it (C.B.)

Received: 20 April 2020; Accepted: 7 May 2020; Published: 9 May 2020


**Abstract:** The Stoddart's blue box (BB) (cyclobis(paraquat-p-phenylene))/iodide binary system was recently demonstrated to give rise to porous three-dimensional networks which can hardly be classified as common XOF-type materials (X = M, C, S, i.e., metal, covalent, or supramolecular organic frameworks), leading to the definition of permutable organized frameworks (POFs). The ternary BB/iodide/iodine system was reported to generate pentaiodide-based structures constituted by the most complex interlocked polyiodides so far isolated (up to an infinite supramolecular pseudopolyrotaxane with a poly[3]catenane axle). The missing link, i.e., the XRD structure of the BB/triiodide complex, is herein reported: structural similarities and novel Raman evidence, opening perspectives in the genesis of solid-state BB-based complex polyiodide networks from solution.

**Keywords:** supramolecular chemistry; polyiodides; Stoddart's blue box; pentaiodide; anion-π interactions; self-assembly

## 1. Introduction

Polyiodide chemistry is a long-lasting research field which, these days, still possesses a theoretical and structural connotation related to bonding theory and hypervalency of polyiodide species [1,2]. At the same time, pragmatic interest in iodine-containing solids, both as crystalline phases and iodine-doped polymers [3,4], has recently re-flourished, especially in view of the potential use of these materials as solid-state electrical conductors [5–7]. Beyond pragmatic interest, studies aimed at selective synthesis of polyiodides [8–11] or at disentangling different stabilizing contributions for these systems [12,13], in view of the recent interest for halogen bonding [14], are also appearing. In this sense, the "feeble force", with which iodides retain molecular iodine in Gay Lussac's writings, appears to have somewhat anticipated whole branches of modern chemistry [1].

Among our recent contributions, we demonstrated the use of tetrazine-based ligands for the coordination of inorganic [15,16] and organic anions [17], emphasizing coordination of halide [18] and pseudohalide anions [19]. Stabilization of anion coordination networks [20], including polyiodide-dense ones [21], has been achieved with s-tetrazine-based ligands through anion-π interactions [22], building on previous evidences of the usefulness of anion-π forces for polyiodide stabilization in perfluoroarene-based systems [23]. We re-evaluated azacyclophanes as templating agents to orchestrate the synthesis of polyiodides: while Ilioudis and Steed [24] reported formation of highly charged polyhalides (e.g., $I_4^{2-}$) with cyclophanes matching the size of iodide anions, we demonstrated that size mismatch can be used to some extent to make the organic ligand act as a mold for the template self-assembly of larger, low-valency polyiodides (e.g., $I_7^-$), leading to extremely iodine-dense crystalline phases [25]; contextually, to benchmark our work with reported literature systems, a novel macroscopic descriptor, the iodine number $I_N$, has been introduced to allow easy comparison of different crystalline materials in terms of iodine density [25].

Our pursuit of highly dense polyiodide-based frameworks and consolidated interest for anion-π interactions eventually led us to consider the organic tetracation cyclobis(paraquat-p-phenylene) (Scheme 1) known as Stoddart's blue box (BB) [26], which is the object of present study. This ligand has initially drawn our attention, as it offers a highly charged scaffold, whose charge is delocalized over a rather large surface: this fixes the number of $I^-$ anions required for charge neutrality to four, without imposing limits on the formal number of $I_2$ molecules that can be co-crystallized; assembly of polyiodides of varying stoichiometries is thus expected, with BB geometry and molecular cavity playing an orchestrating role.

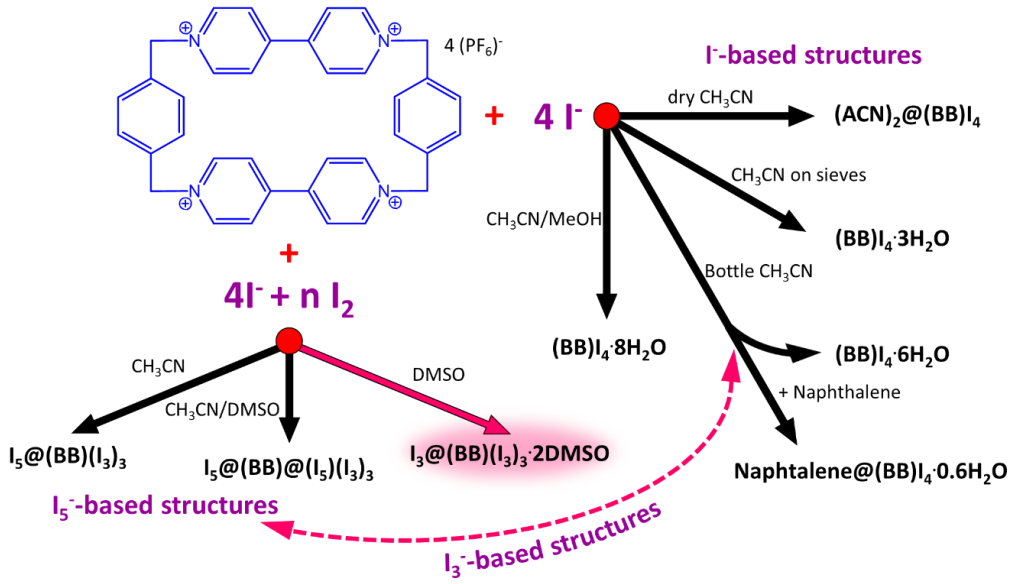


**Scheme 1.** Overview of reported crystalline phase for the binary blue box (BB)/$I^-$ [27] and ternary BB/$I^-$/$I_2$ [28] systems. The two subgroups of $I^-$- and $I_5^-$-based structures were hardly relatable, due to the lack of an intermediate $I_3^-$-based architecture. The $I_3$@(BB)$(I_3)_3$·2DMSO crystal structure herein reported fills the gap allowing substantial comparison of packing features. Adapted from [27] with permission from John Wiley and Sons.

The BB/$I^-$ binary system has been recently investigated, leading to interesting findings [27].

Robustness, due to charge-charge attraction, and flexibility, due to reduced directionality of BB ··· $I^-$ interactions, led to the preparation of a novel type of porous networks named permutable organized frameworks (POFs) [27]. POFs feature a 3D hollow architecture held together by supramolecular ball joints, which allow for different mutual orientation of constituents in the solid, granting the network a flexibility which is generally made impossible by design for the rigid jointed metal organic frameworks (MOFs), covalent organic frameworks (COFs), and supramolecular organic frameworks (SOFs) (generally based around strictly directional H-bonds) [27].

The ternary BB/$I^-$/$I_2$ system led instead to the formation of some of the more intricate, and arguably charming, polyiodide architectures of all time [28].

In fact, $I_5$@(BB)$(I_3)_3$ crystal structure features a peculiar infinite supramolecular [3]catenane constituted by 14-membered $I_5^-$ rings interlocked with two BB molecules each. By tuning crystallization conditions, i.e., fostering the conversion of a further $I_3^-$ anion into a second $I_5^-$, the $I_5$@BB@$(I_5)(I_3)_2$ crystal structure is obtained, where the infinite [3]catenane is converted into the axle of an infinite supramolecular pseudopolyrotaxane, where the "macrocyclic" components are $(I_5)_2(I_3)_4$ 22-membered polyiodide rings [28]. It is noteworthy that, while being both mixed $I_3^-$/$I_5^-$ complexes, the core $(I_5$@BB$)_\infty$ [3]catenane is the cornerstone of these structures and passes unmodified from one structure to the other.

Here, we present the missing link between the five reported BB/$I^-$ crystal structures and the two mixed BB/$I_3^-$/$I_5^-$ crystals, i.e., a structure featuring only triiodide as anion. As we show, this structure

features analogies with both families of $I^-$- and $I_5^-$-based crystal structures reported so far, and it is especially relevant for the understanding of the genesis of these crystalline phases.

## 2. Materials and Methods

$I_3$@BB$(I_3)_3$·2DMSO crystals were obtained by leaving exposed to the air a DMSO solution of BB$(PF_6)_4$ containing 1:2 mol:mol NaI and $I_2$. Alternatively, $I_3$@BB$(I_3)_3$·2DMSO were obtained by dissolving $I_5$@BB$(I_3)_3$ crystals [28] in DMSO and waiting for subsequent spontaneous crystallization (see Section 3.4). Both methods are quite slow and required several (7–10) weeks. All employed materials were high purity commercial products.

Black crystals of $I_3$@BB$(I_3)_3$·2DMSO were used for X-ray diffraction analysis. A summary of the crystallographic data is reported in Table S1. The integrated intensities were corrected for Lorentz and polarization effects, and an empirical absorption correction was applied [29]. The structure was solved by SHELXS-97 [30]. Refinements were performed by means of full-matrix least-squares, using SHELXL Version 2014/7 [30].

Raman spectra of $I_5$@BB$(I_3)_3$ and $I^-/I_2$ DMSO solutions were recorded with a Brucker FT-Raman Multiram spectrometer equipped with a Nd-YAG laser emitting at 1064 nm as excitation source. The spectra were recorded on solid DMSO-wetted $I_5$@BB$(I_3)_3$ as it gradually dissolved, giving a DMSO solution of BB-polyiodide complexes. Acquisition settings were: 4 $cm^{-1}$ resolution, 150 mW incident power, 50 acquisition scans. Recrystallization of $I_3$@BB$(I_3)_3$·2DMSO crystals happened spontaneously over time from these solutions.

Data analysis and graphical presentation was performed with CCDC Mercury [31] and CrystalExplorer [32] software.

## 3. Results and Discussion

### *3.1. $I_3$@BB$(I_3)_3$·2DMSO*

Evaluated in isolation, the $I_3$@BB$(I_3)_3$·2DMSO crystal structure can be described as a piling of BB molecules in pillars along the *a* direction. Pillars are held together by two of the four non-equivalent $I_3^-$ anions located along the widest (paraquat) BB side (Figure 1).

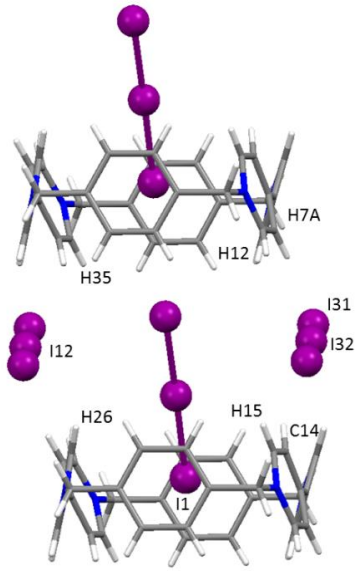


**Figure 1.** Column of macrocycles and triiodides growing in the *a* crystallographic direction in the $I_3$@BB$(I_3)_3$·2DMSO crystal structure.

A third $I_3^-$ is found to occupy the pillar cavity, hosting one of its I atoms within the BB frame. As a result, looking along the *a* direction, a wire of triiodides passing through BB molecules spans

the whole crystal. The fourth non-equivalent $I_3^-$ anion is also organized in wires passing in between adjacent BB pillars. Figure 2 offers a complete view of the crystal packing. Contact distances according to the labelling scheme of Figures 1 and 2 are reported in the Supplementary Materials (Table S2).

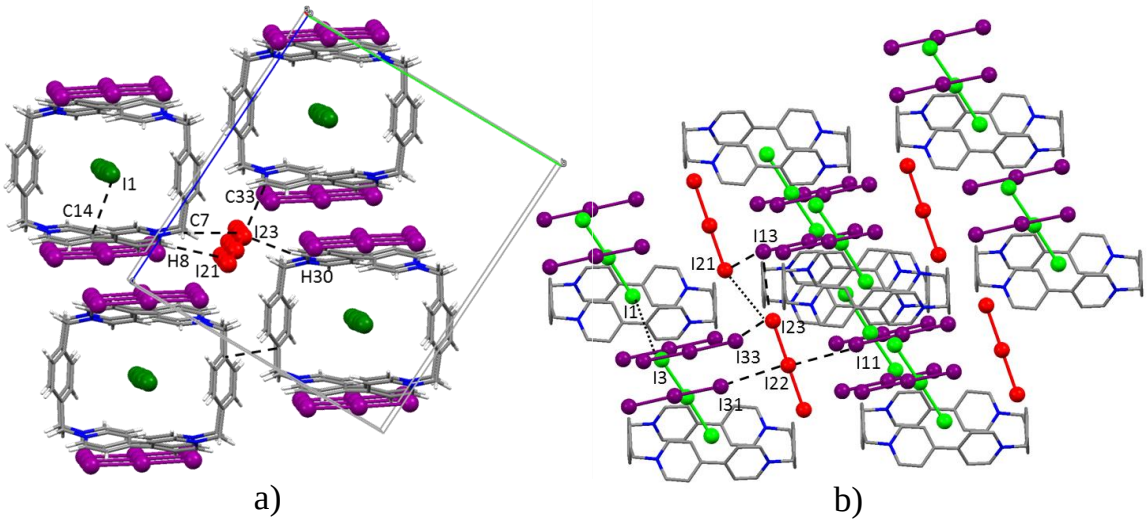


**Figure 2.** $I_3$@BB$(I_3)_3$·2DMSO crystal structure. Top view (**a**) and lateral view (**b**) of the BB/$I_3^-$ pillars growing along the *a* axis. Color code: purple: triiodides bridging piled BB; green: triiodides inside the BB cavity; red: triiodides outside the BB pillars. DMSO molecules omitted for clarity. I ··· I, C ··· I, and H ··· I contacts as dashed lines.

The result is that of a highly dense polyiodide network ($I_N$ = 0.354, i.e., ≈ $^1/_3$ of the iodine density of crystalline $I_2$ [25]). Differently from $I_5^-$-based crystal structures, however, we observe the lack of short I ··· I supramolecular contacts among individual $I_3^-$: the shortest one being 4.2834(5) Å (I13 ··· I21). This implies the lack of maintenance of orbital contact and the consequent impossibility of the $I_3$@BB$(I_3)_3$·2DMSO structure to exhibit any conductive behavior [28].

Arguably, however, the most interesting approach for examining this structure includes its comparison with $I^-$- and $I_5^-$-based ones.

### 3.2. Structural Comparison

The family of $I^-$-based structures, obtained from acetonitrile (ACN) solvent, was found to exhibit a ball-and-socket joint architecture, where spherical iodide anions occupy preferentially BB aromatic corners, the charge-assisted CH ··· I contacts are more favorable, and maintain a degree of angular freedom in the direction of pillar growth [27]. A major exception to this is constituted by the (BB)$I_4$·8$H_2O$ structure, where, due to the higher polarity of the solvent (ACN/MeOH, Scheme 1), burrowing of $I^-$ anions inside the BB was observed [27].

According to these observations, the prototypical $(ACN)_2$@(BB)$I_4$ crystal structure, and the abovementioned (BB)$I_4$·8$H_2O$ [27], result as the most relevant $I^-$-based structures to compare with $I_3$@BB$(I_3)_3$·2DMSO.

As can be seen from Figure 3, the terminal atoms of the two $I_3^-$ anions responsible for intra-pillar BB ··· BB bridging in the $I_3$@BB$(I_3)_3$·2DMSO structure occupy almost the same spots of simple $I^-$ anions in the $(ACN)_2$@(BB)$I_4$ crystal, most likely due to a fortunate coincidence between the length of $I_3^-$ anion and the spacing of BB CH binding sites. Triiodides are found slightly more detached from BB than iodide anions, however this could be expected due to change in the anion charge density affecting the strength of charge-charge interactions. As shown in Figure 3, the pillar step, in terms of BB ··· BB distance, is basically unaffected, while a certain adjustment of the pillar growth angle is observed: this type of flexibility is a leitmotiv of $I^-$-based structures [27].

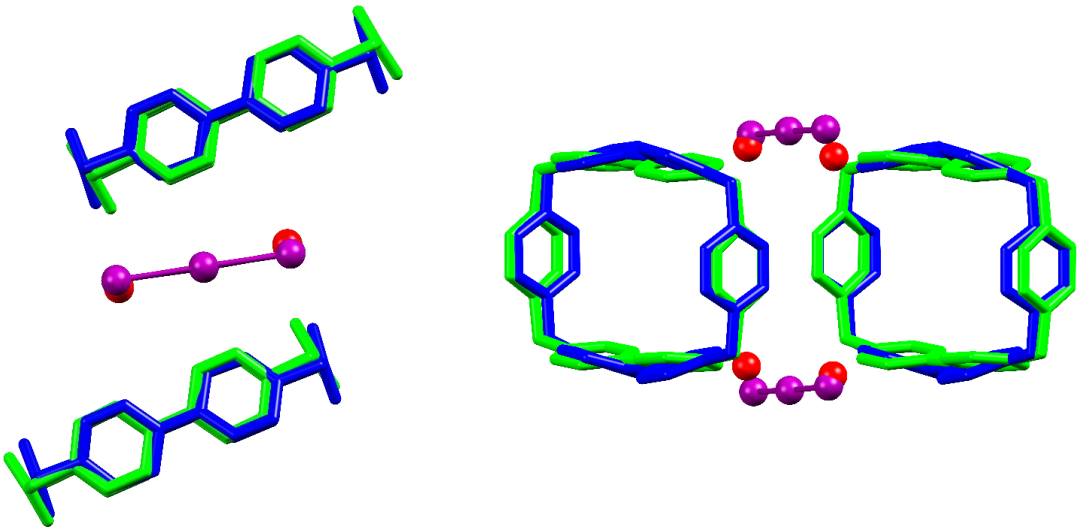

**Figure 3.** Side and top view of $I_3$@BB$(I_3)_3$·2DMSO structure (in blue and violet ($I_3^-$)) superimposed to $(ACN)_2$@$(BB)I_4$ (in green and red ($I^-$)). Superimposition obtained by overlap of the eight C atoms of BB methylenic corners (RMS = 0.383).

The $(BB)I_4·8H_2O$ crystal structure allows instead for comparison of the mutual positions of BB and hosted $I^-$ or $I_3^-$ anion. As shown in Figure 4 for both non-equivalent BB molecules found in $(BB)I_4·8H_2O$ (termed molecule A and molecule B) [27], it is observed that the position occupied by the iodide anion is almost coincident with the position of the central atom of the triiodide. This does not appear fortuitous, as this atom is formally the charge-bearing one, indicating that the charge-charge component of the piridinium-$I_3^-$ anion-π contact is the most significant for the host-guest interaction.

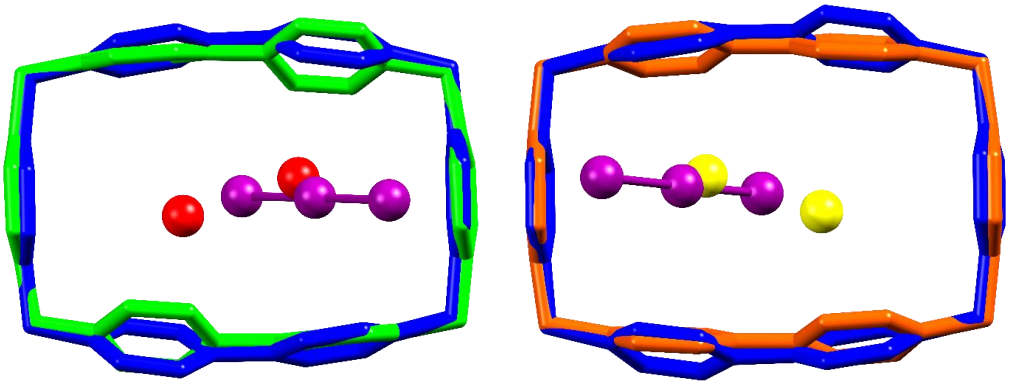

**Figure 4.** Comparison of host-guest interaction for BB ··· $I_3$ in $I_3$@BB$(I_3)_3$·2DMSO (blue and violet) and BB ··· $I^-$ in $(BB)I_4·8H_2O$ (green and red: molecule A; orange and yellow: molecule B). Superimposition obtained by overlap of the four C atoms of BB methylenic corners (RMS = 0.110 and 0.057 for molecule A and B, respectively).

As can be concluded from the above examination, the main differences between $I_3^-$- and $I^-$-based structures are not to be ascribed to significant differences in the BB pillar motif or in the host-guest interactions. The main factor in play appears to be tied to charge balance and anion size reasons. Four $I^-$ per BB were required to hold together the BB pillars in the prototypical $(ACN)_2$@$(BB)I_4$ crystal structure, yet the same structural role can be fulfilled by only two $I_3^-$ anions (as displayed in Figure 3), thus leaving two BB positive charges to be counterbalanced. One of these charges is provided by the encapsulated $I_3^-$ anion; this again shows similarity with BB-$I^-$ host-guest complex, as found in $(BB)I_4·8H_2O$ (Figure 4). In the case of $(BB)I_4·8H_2O$, two $I^-$ anions could be accommodated within the cavity, yet, as manifest from Figure 4, maintenance of the position of the negative charge inside the

cavity, and the $I_3^-$ increased size, prevent accommodating two negative charges within each BB in the case of $I_3$@BB$(I_3)_3$·2DMSO. This leaves a last +1 charge to be compensated. The line of triiodides passing in between adjacent BB pillars (Figure 2, red) is thus the most noticeable distinguishing element between the $I_3$@BB$(I_3)_3$·2DMSO crystal structure and $I^-$-based ones, and it is brought about not by a difference in interactions subtending to $I_3^-$ and $I^-$ BB complexes, but by the necessity of accommodating a fourth negative charge per BB molecule.

This same argument can be raised also in the comparison with $I_5^-$-based structures.

In fact, as displayed in Figure 5, these structures feature coupled BB pillars held together by $I_5 \cdots I_5$ interactions and $\pi$-$\pi$ stacking forces [28].

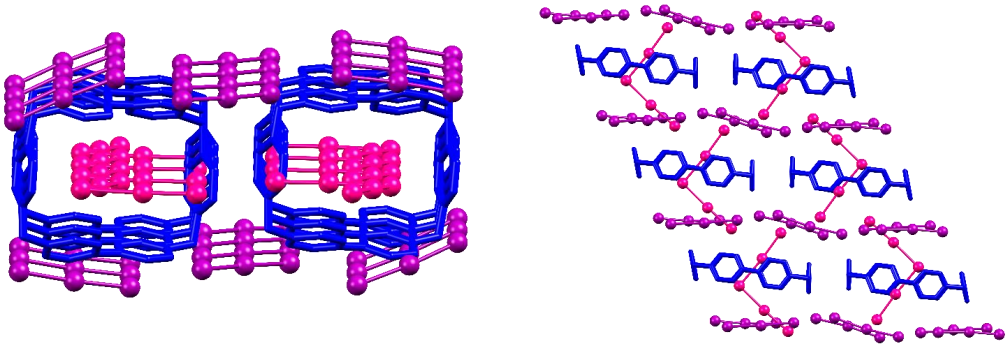

**Figure 5.** Front and top view of coupled BB pillars as found in the $I_5$@(BB)$(I_3)_3$ crystal structure.

If, as shown in Figure 3, pillars formed by piling of one BB above another can be stabilized either by two triiodides or four iodides acting as bridging elements, coupled BB pillars as found in $I_5^-$-based structures are too large for that, requiring a total of six triiodides to bridge each coupled BB complex with the next one. In terms of charges, for each two BB molecules (+8), a total of six triiodides is required (−6), leaving a +2 charge to be counterbalanced, which is easily achieved by the presence of the $I_5^-$ anions within the BB cavity (one for each) (which in turn is the very reason for coupling of BB pillars).

Again, the presence of a second line of polyiodides spanning the crystal beyond the one passing through BB cavities is entirely unique of $I_3$@BB$(I_3)_3$·2DMSO, and due to charge balance reasons. All the other architectures use as many iodide or triiodide anions as required to stabilize intra-pillar piling of BB molecules and place the remaining anions within the ligand cavity. Only for $I_3$@BB$(I_3)_3$·2DMSO, when this process is repeated, are additional anions required for charge neutrality, leading to a train of polyiodides passing in between different BB pillars.

Conversely, the core architecture of iodide/polyiodide-stabilized BB pillars, together with main supramolecular interactions subtending to it, is essentially preserved from one structure to another. Despite different space groups and contents of the asymmetric unit, all systems present a lattice vector directed along the BB pillars' growth direction of invariant modulus ($(ACN)_2$@(BB)$I_4$, *b*, 10.5041(2) Å; $I_3$@BB$(I_3)_3$·2DMSO, *a*, 10.3559(6) Å; $I_5$@(BB)$(I_3)_3$, *a*, 10.3325(2) Å), signifying the presence of a characteristic interaction pattern beyond the specificity of each crystal packing.

Comparison with $I_5^-$-based structures, specifically with prototypical $I_5$@(BB)$(I_3)_3$, can also be undertaken in terms of host-guest complex structural features.

This time, the BB-anion's mutual disposition between $I_3^-$ and $I_5^-$ are different, and tellingly similar at the same time (Figure 6).

As is well-known, $I_5^-$ can exist in a symmetric V-shaped form, rationalized as an $[(I_2)\cdot(I^-)\cdot(I_2)]$ complex formally charged on the central atom, or in a L-shaped form, schematized as an $[(I_3^-)\cdot(I_2)]$ complex with the charge localized on one of the proximal I atoms [2,21]. Both forms are frequently occurring in the solid state, and proper assignment is generally a focal point for case-by-case assessment of $I_5^-$ electronic structure [2]. This point has been previously investigated for $I_5$@(BB)$(I_3)_3$; as demonstrated by reported Raman spectra of DMSO-soaked $I_5$@(BB)$(I_3)_3$ (solvent is necessary to

avoid immediate radiation damage on the crystals preventing recording of any spectrum [28], cf. Section 3.4), in this case $I_5^-$ is observed to be in the fully symmetric V-form.

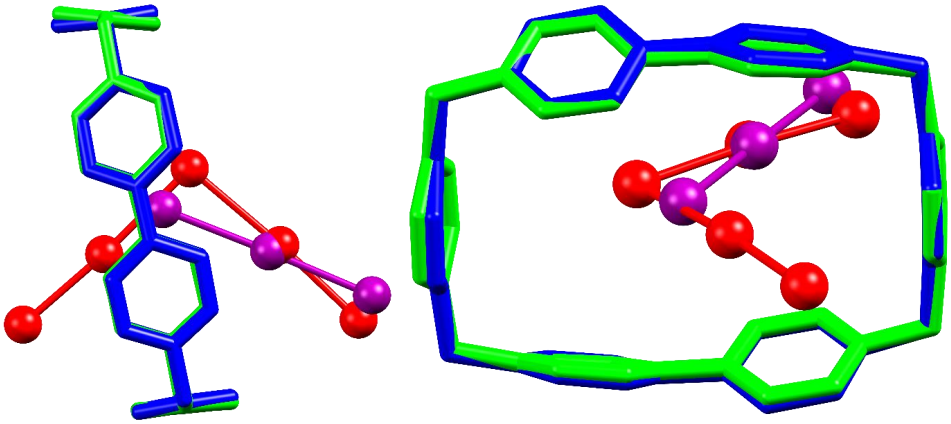

**Figure 6.** Side and front comparisons of host-guest interaction for BB $\cdots$ $I_3$ in $I_3$@BB$(I_3)_3$·2DMSO (blue and violet) and BB $\cdots$ $I_5^-$ in $I_5$@(BB)$(I_3)_3$ (green and red). Superimposition is obtained by overlap of the four C atoms of BB methylenic corners (RMS = 0.0617).

What we are now able to notice from crystal structure superimposition is that, if on one hand there is no atom by atom coincidence, still the position of the central formally charge-bearing atom of $I_3^-$ is relatively close not to the central $I_5^-$ atom, as would be expected if it were charge-bearing, but to one of the proximal I atoms. Since the position of BB encapsulated charge-bearing I atoms was found not to differ much also in the $I^-$-based structures, where charge localization is straightforward, it could be argued whether observed V-symmetry for $I_5^-$ in $I_5$@(BB)$(I_3)_3$ is tied to intrinsic preferences of the BB-$I_5^-$ host-guest complex, or rather due to the tight network of $I_5^-$-$I_5^-$ interactions within the crystal (Figure 5). As a matter of fact, this led us to seek further Raman evidence for $I_5^-$ complexation in solution, where it could be possible to obtain information on the isolated (solvated) $I_5^-$@BB complex and assess the V- or L-shaped nature of the anion (see Section 3.4).

### *3.3. Hirshfeld Surface Analysis*

Hirshfeld surface can be defined in plain words as the region of space where the electron distribution of a theoretical collection of spherical atoms, representing the molecule under discussion (the promolecule), dominates the corresponding summation over the whole crystal depicted in the same manner (the procrystal): mathematical definition, properties, and usefulness of Hirshfeld surface are found in dedicated literature [33,34]. This allows for a comprehensive and "non-biased" (in the sense that it does not involve choices concerning what is deemed important and worth discussing and what is not) evaluation of all contacts within a crystal structure. Moreover, the same treatment allows for the visualization of a crystal structure through the lens of so-called fingerprint plots [35]. These are complete maps of external distance ($d_e$) (i.e., the point-by-point distance of the nearest atom belonging to another molecule to the Hirschfeld surface of considered species) vs. internal distance ($d_i$) (i.e., the point-by-point distance from a molecule's Hirshfeld surface and the nearest atom belonging to the molecule itself) from the Hirshfeld surface under consideration, color-coded to show relative abundance (from blue: few contacts, to red: many contacts) of intermolecular contacts occupying $d_i \times d_e$ square bins of $0.01 \times 0.01$ Å$^2$.

These tools were developed to obtain a comprehensive view of a crystal and assist in formalizing and quantifying concepts like similarity among different crystal structures. In a previous study, we demonstrated how such an approach is of particular significance in our case, as crystal structures generated by the BB/$I^-$/$I_2$ ternary system all develop about a single invariant molecular component (BB), around which the whole crystal architecture unfolds [27]. This allows us to directly compare these structures through this methodology.

Results of the analysis for $(ACN)_2$@(BB)$I_4$, $I_3$@(BB)$(I_3)_3$·2DMSO and $I_5$@(BB)$(I_3)_3$ crystal structures are reported below in Figures 7 and 8.

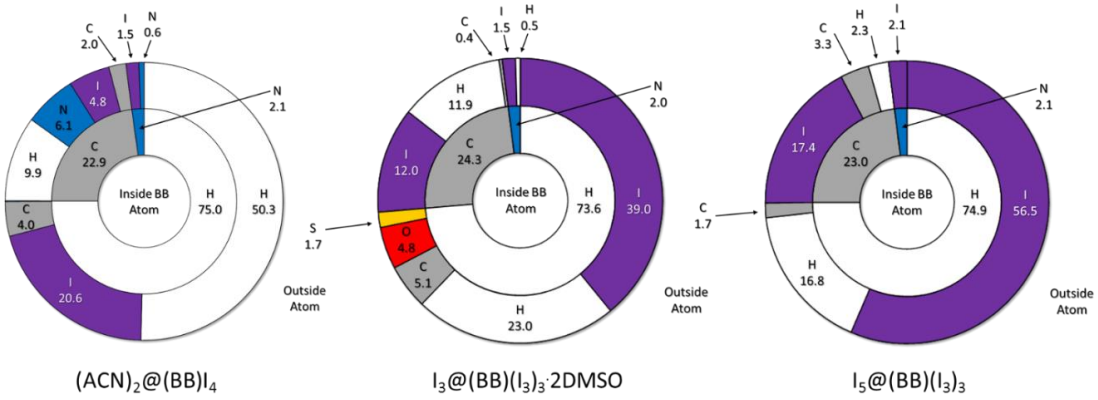


**Figure 7.** Overview of BB Hirshfeld surface composition for all discussed crystal structures (same data in tabular form are found in Table S3). Inner ring: internal composition of Hirshfeld surface, i.e., a depiction of BB molecular surface; outer ring: closest outer atom, i.e., atom in contact with BB Hirshfeld surface. Color code: white: H; grey: C; blue: N; red: O; yellow: S; violet: I. Data from $(ACN)_2$@(BB)$I_4$ crystal structure taken from [27]. Partly adapted from [27] with permission from John Wiley and Sons.

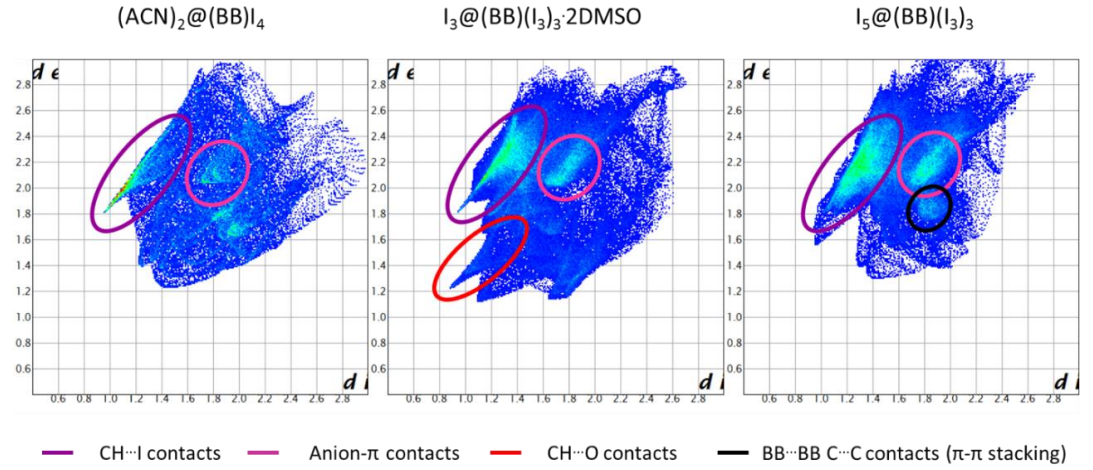


**Figure 8.** Overview of BB fingerprint plots for all discussed crystal structures. A breakdown of assignment of recognizable features is presented in Figure S1. Partly adapted from [27] with permission from John Wiley and Sons.

The main observation from Hirshfeld surface composition (Figure 7) is the progressive increase of BB ··· I contacts with increasing I content (or iodine number, $I_N$ = 0.154, 0.354, and 0.447, for considered $I^-$, $I_3^-$, and $I_5^-$ based structures, respectively). This might seem unsurprising, yet fingerprint plots allow evidence for a certain change in the type of BB ··· I main interactions.

As shown in Figure 8, and better detailed in Figure S1, in the case of $(ACN)_2$@(BB)$I_4$, main BB ··· I contacts are of the H ··· I type, giving rise to the classic tip-like feature expected for H-bond type interactions. A minor contact-dense zone related to C ··· I, i.e., pyridinium-$I^-$ anion-π interaction, is also manifest [27]. As we move towards polyiodide-based structures, the predominance of CH ··· I contacts and H-bonds is gradually reduced, together with the anion charge density. Polarizability and size of the anion increases, and so does the relevance of stabilizing contributions that can take advantage of it; in this case, anion-π interactions. The defined sharp H-bond tip observed for H ··· I contacts in $(ACN)_2$@(BB)$I_4$ gets smeared and blurred the more we move towards $I_5$@(BB)$(I_3)_3$, while at the same time, the relevance of anion-π contacts, just glimmering in the $(ACN)_2$@(BB)$I_4$ fingerprint,

become a major feature. $I_3$@BB$(I_3)_3$·2DMSO indeed appears as a bridging instance between these two different trends, showing similarities with both $I^-$ and $I_5^-$-based structures.

Another point worth mentioning is the extent of BB ··· BB face-to-face π-π stacking. This is absent in the case of the $(ACN)_2$@$(BB)I_4$ structure (C ··· C contacts in Figure S1 are entirely due to host-guest C ··· C contacts between ACN and hosting BB molecule), barely present in $I_3$@BB$(I_3)_3$·2DMSO, and relevant for $I_5$@$(BB)(I_3)_3$. This is due to the abovementioned coupling of BB pillars existing in $I_5^-$ structures (both $I_5$@$(BB)(I_3)_3$ and $I_5$@BB@$(I_5)(I_3)_2$) and, judging from the invariance of the core $(I_5$@$BB)_\infty$ [3]catenane from one structure to another, most likely points out the stability of such an arrangement (also consolidated by $I_5^-$ ··· $I_5^-$ interactions, cf. Figure 5). This view is experimentally supported by TGA analysis of $I_5$@$(BB)(I_3)_3$ crystals, showing loss of the first $I_2$ molecule only beyond 110 °C [28].

### *3.4. Raman Evidence*

Direct Raman spectroscopic investigation of $I_3$@BB$(I_3)_3$·2DMSO crystals was not possible, due to the same issues affecting $I_5$@$(BB)(I_3)_3$ crystals (strong radiation absorption resulting in crystal damage).

The lack of coincidence between charge-bearing atoms for BB-hosted $I_3^-$ and $I_5^-$ in the crystal structure (cf. Figure 6 and related discussion) sheds doubt over pentaiodide geometry/electronic structure. V-shaped symmetry substantiated for pentaiodide in $I_5$@$(BB)(I_3)_3$ could be due to packing features (cf. Figure 5) [28] and is not conclusive for the isolated $I_5^-$@BB host-guest complex; therefore, further Raman investigation in solution was performed.

This was done starting from $I_5$@$(BB)(I_3)_3$ crystals because they are DMSO soluble (differently from $I_3$@BB$(I_3)_3$·2DMSO crystals, which moreover are obtained by letting these solutions crystallize).

In reconsidering the matter, interesting pieces of evidence emerge.

Despite a long literature tradition of dismissing the matter by saying that $I_5^-$ is never present in solution [36], we, as others before us [37], were able to show that free $I_5^-$ exists in solution. This was done by preparing 1:2 NaI:$I_2$ DMSO solutions and recording their Raman spectra. As it can be seen in Figure 9, a clear $I_5^-$ band centered at 170 $cm^{-1}$ becomes more and more manifest the more $I_5^-$ formation in solution is forced by mass action (minor shift of neighboring bands is also observed); assignment of observed bands is reported in Table 1.

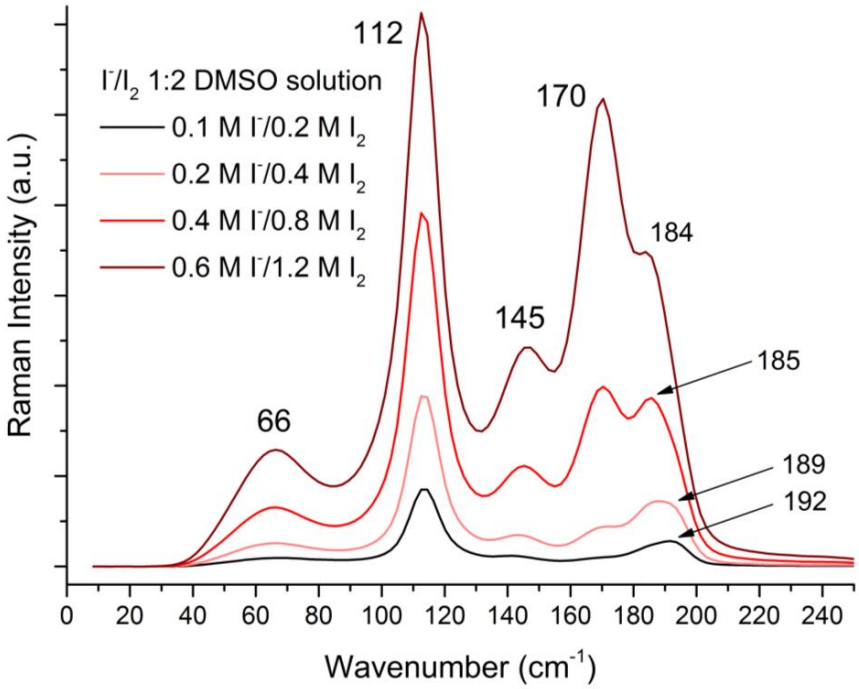


**Figure 9.** Raman spectra of DMSO $I^-/I_2$ 1:2 solutions at different concentrations showing the concentration-dependent presence of a strong band at 170 $cm^{-1}$, diagnostic of V-shaped $I_5^-$.

**Table 1.** Breakdown and assignment of Raman bands observed in Figure 9.

| $I_2$ | $I_3^-$ | $I_5^-$ | Assignment |
|---|---|---|---|
| | 66 m | | bending $v_2$ |
| | 112 vs | | symmetric stretch $v_1$ |
| | 145 m | | asymmetric stretch $v_3$ |
| | | 170 s | symmetric stretch V-shaped |
| 192 m | | | Symmetric stretch $v_1$ |

The observed $I_5^-$ symmetric stretch vibration frequency perfectly corresponds to literature values for symmetric V-shaped $I_5^-$ [2], indicating that $I_5^-$ solvation in DMSO can be considered isotropic, or at least isotropic enough not to cause a significant distortion of the anion converting it in its L shape. Proper determination of an equilibrium constant for the $I_3^- + I_2 = I_5^-$ was not possible, due to deviation from ideality and non-linear response of the Raman signal in solutions of such high concentration; however, observation of spectral changes only at sub-molar concentration are in agreement with reported very small *K* values (log $K \approx 1$ in water [37]).

Raman spectra of the DMSO-soaked $I_5$@(BB)$(I_3)_3$ were re-recorded in the very same manner as in [26] and showed analogous results. This time, however, spectra were recorded from the initial wetting of the crystals for up to 30 min (after which no further changes were observed) while crystal dissolution in DMSO proceeded; data are reported in Figure 10.

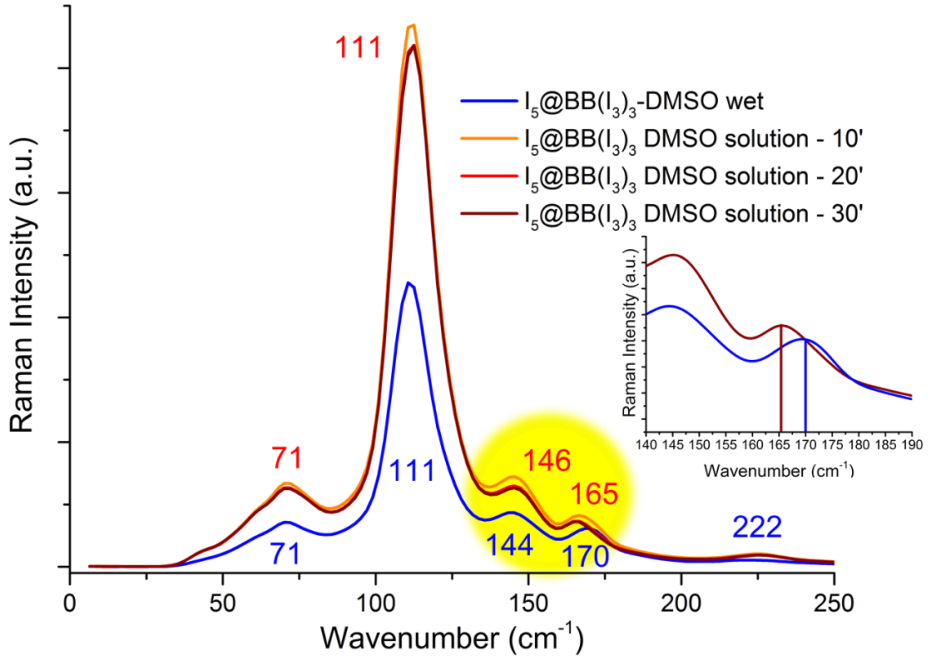


**Figure 10.** Variation of Raman spectra as $I_5$@(BB)$(I_3)_3$ slowly dissolves in DMSO.

Beyond a difference in intensity caused by the dissolution process, all bands remained at the same frequencies except the one related to $I_5^-$ stretching. For tiny the shift of $I_5^-$ vibration frequency may seem, it cannot be overlooked, as it actually covers the whole expected literature range of variability from a perfectly V-shaped (170 $cm^{-1}$) to a markedly L-shaped (165 $cm^{-1}$) pentaiodide [2].

Since we demonstrated that pentaiodide is V-shape symmetrical in DMSO in the absence of ligand, as well as in the $I_5$@(BB)$(I_3)_3$ crystal (both from Raman spectra, Figure 10 blue line, and crystal data: central I-I 3.076(1)-3.139(1) Å, distal I-I 2.805(2)–2.785(1) Å, angle 94.54(4)°), its observed transition to L-shaped form must be assigned to discrete [$(I_3^-)\cdot(I_2)$]@BB host-guest complexes, which exist as isolated entities in solution.

It becomes clear that parameters affecting polyiodide formation equilibria ($I^- + I_2 = I_3^-$, $I_3^- + I_2 = I_5^-$, etc.), among which the choice of the solvent plays a fundamental role, have a deep influence on the resulting crystal packing for the BB/$I^-$/$I_2$ ternary system.

It can be concluded that a fine game of equilibria, perhaps not fully understood due to the limits imposed by solubility (all $I^-$ and $I_5^-$ structures are obtained from acetonitrile, a solvent eluding direct investigation due to complexes extreme insolubility), subtends to the formation of these systems.

Both $I_3^-$ and $I_5^-$, as demonstrated by crystal structures, can be hosted within BB cavities. Such host-guest interaction exists also in DMSO solution and causes a reduction of symmetry of $I_5^-$ anions. Due to the stability of the $(I_5@BB)_\infty$, it is possible for discrete $I_5^-$@BB complexes to associate, giving a crystalline solid, where $I_5^-$ regains its V-shaped symmetry due to additional $I_5^- \cdots I_5^-$ contacts. The solvent of choice must implicitly play a major role by affecting the position of $I_3^- + I_2 = I_5^-$ equilibrium, this being most likely the reason for the impossibility to isolate $I_5^-$-based crystals from DMSO, while their formation is commonplace in ACN.

## 4. Conclusions

The $I_3@BB(I_3)_3{\cdot}2DMSO$ crystal structure represents an important conceptual link between reported $I^-$- and $I_5^-$-BB-based architectures. Accordingly, it allows for a broad rationalization of the most important phenomena governing the formation of these systems.

In the first place, the original idea of having a large charged scaffold imposing limits on the number of required iodide anions, but not on the number of formal additional $I_2$ molecules, indeed resulted in systems which are interesting and intricate at the same time. In particular, charge balance is at the core of some of the major differences observed among these structures.

For the BB/$I^-$ family of structures, as manifest from Figure 7, the role of charge-charge interactions is fundamental and leads to four multiple CH $\cdots$ I contacts, exploiting BB corners, which are responsible for holding together BB pillars and balancing out the BB charge.

The BB/$I_5^-$ family of structures seems to be dominated by the stability of the $(I_5^-@BB)_\infty$ [3]catenate, that passes unmodified from one structure to the other. The main type of forces in play in this type of structure are of the anion-$\pi$ type, according to the polarizability of both BB and larger polyiodides. The other three required charges are provided by three almost aligned $I_3^-$ anions, which are just big enough to bridge the BB coupled pillars brought about by the core [3]catenane architecture.

The $I_3@BB(I_3)_3{\cdot}2DMSO$ is a mix of both trends. It maintains BB $\cdots$ I corner contacts as in $I^-$-based structure, though requiring only two $I_3^-$ to bridge a pair of adjacent BB molecules, rather than four $I^-$. At the same time, $I_3^-$, due to its large surface allowing for multiple contacts, is more easily stabilized than $I^-$ within the BB cavity (yet not as much as $I_5^-$). One last charge remains to be counterbalanced, giving rise to a line of triiodides passing in between pillars: a feature unique to this structure.

The second focal point regards the role of the solvent and its importance for the position of the $I_3^- + I_2 = I_5^-$ equilibrium in solution, which in turn is crucial to determine which polyiodide architecture is formed.

As a matter of fact, from ACN solvent it is possible to obtain an $I^-$-based structure in absence of $I_2$ or $I_5^-$ based structures in the presence of $I_2$, while stopping at phases containing only $I_3^-$ is not observed. The fact that $I_3@BB(I_3)_3{\cdot}2DMSO$ is obtained from the same solvent (DMSO) that was used for Raman investigation of $I_5@(BB)(I_3)_3$ prompted further study. It was found that the symmetric V-shaped $I_5^-$, as found in $I_5@(BB)(I_3)_3$, shifts to an L-shaped $I_5^-$ in DMSO solution, due to host-guest interactions with BB which reduce its symmetry.

This indicates that when the choice of solvent is such to allow compresence of $I_5^-$ and BB in solution over a certain threshold, monomeric $I_5^-$@BB host-guest complexes present in solution start interacting and form inevitably the very stable $(I_5^-@BB)_\infty$ [3]catenate, leading to $I_5^-$-based architectures. Conversely, the more the solvent favors $I_5^-$ dissociation, the more the process becomes unlikely, allowing for the formation of $I_3^-$-based phases. In the case of DMSO, even starting from 1:2 $I^-$:$I_2$ solutions does not lead to $I_5^-$-containing structures; this appears indicative of the ability of

DMSO to dissociate $I_5^-$ more effectively in comparison to ACN; in turn this being probably the reason underlying to the solubility of $I_5^-$-based crystals in DMSO.

In the end, given on one hand the interest for $I_2$-dense solids for solid-state conductor applications [5–7], and on the other one, the recent demonstration of the usage of $I^-$ anions as supramolecular ball joints, leading to a new class of porous materials, POFs, whose structure is inherently dependent on crystallization conditions [27], we can anticipate that fine understanding of the "homeostasis" of polyiodides in the BB/$I^-$/$I_2$ system will be a guiding light in the design of related materials intended for applications.

**Supplementary Materials:** The following are available online at http://www.mdpi.com/2073-4352/10/5/387/s1, Table S1: Crystallographic information; Table S2: Selected contacts for the $I_3$@BB$(I_3)_3$·2DMSO crystal structure; Table S3: Overview of BB contacts in the examined crystal structures according to Hirshfeld surface analysis; Figure S1: Synopsis of fingerprint plots. CCDC deposition number 1996957 contains the supplementary crystallographic data for this paper. These data can be obtained free of charge via http://www.ccdc.cam.ac.uk/conts/retrieving.html.

**Author Contributions:** Conceptualization: A.B.; methodology: all authors; validation: C.B. and C.G.; formal analysis: all authors; investigation: C.B., C.G., and M.S.; resources: A.B., C.B., and C.G.; writing—original draft preparation: M.S.; writing—review and editing: all authors; visualization: M.S.; supervision: A.B. and C.B.; project administration: A.B.; funding acquisition: A.B. and C.B. All authors have read and agreed to the published version of the manuscript.

**Funding:** This research received no external funding.

**Acknowledgments:** CRIST, Crystallography Centre, University of Florence, is gratefully acknowledged for technical support.

**Conflicts of Interest:** The authors declare no conflicts of interest.

## References and Note

1. Gay-Lussac, J.L. Mémoire sur l'iode. *Ann. Chimie* **1814**, *91*, 5–160.
2. Svensson, P.H.; Kloo, L. Synthesis, structure, and bonding in polyiodide and metal iodide-iodine systems. *Chem. Rev.* **2003**, *103*, 1649–1684. [CrossRef] [PubMed]
3. Reiss, G.J.; van Megen, M. Two new polyiodides in the 4,4′-bipyridinium diiodide/iodine system. *Zeitschrift Für Naturforschung B* **2012**, *67*, 5–10.
4. Van Megen, M.; Reiss, G.J. The pseudosymmetric structure of bis(pentane-1,5-diaminium) iodide tris(triiodide). *Acta Cryst. E* **2012**, *68*, o1331–o1332. [CrossRef] [PubMed]
5. Li, J.; Wang, Z.-S. Lithium-coordinating ionic conductor for solid-state dye-sensitized solar cells. *RSC Adv.* **2015**, *5*, 56967–56973. [CrossRef]
6. Wang, H.; Li, J.; Gong, F.; Zhou, G.; Wang, Z.-S. Ionic Conductor with High Conductivity as Single-Component Electrolyte for Efficient Solid-State Dye-Sensitized Solar Cells. *J. Am. Chem. Soc.* **2013**, *135*, 12627–12633. [CrossRef] [PubMed]
7. Wang, H.; Li, H.; Xue, B.; Wang, Z.; Meng, Q.; Chen, L. Solid-State Composite Electrolyte LiI/3-Hydroxypropionitrile/$SiO_2$ for Dye-Sensitized Solar Cells. *J. Am. Chem. Soc.* **2005**, *127*, 6394–6401. [CrossRef]
8. Svensson, P.H.; Gorlov, M.; Kloo, L. Dimensional caging of polyiodides. *Inorg. Chem.* **2008**, *47*, 11464–11466. [CrossRef]
9. Abate, A.; Brischetto, M.; Cavallo, G.; Lahtinen, M.; Metrangolo, P.; Pilati, T.; Radice, S.; Resnati, G.; Rissanen, K.; Terraneo, G. Dimensional encapsulation of $I^-\cdots I_2\cdots I^-$ in an organic salt crystal matrix. *Chem. Commun.* **2010**, *46*, 2724–2726. [CrossRef]
10. García, M.D.; Martí-Rujas, J.; Metrangolo, P.; Peinador, C.; Pilati, T.; Resnati, G.; Terraneo, G.; Ursini, M. Dimensional caging of polyiodides: Cation-templated synthesis using bipyridinium salts. *CrystEngComm* **2011**, *13*, 4411–4416. [CrossRef]
11. Lin, J.; Martí-Rujas, J.; Metrangolo, P.; Pilati, T.; Radice, S.; Resnati, G.; Terraneo, G. Solution and Solid State Synthesis of the Discrete Polyiodide I73– under Modular Cation Templation. *Cryst. Growth Des.* **2012**, *12*, 5757–5762. [CrossRef]
12. Peuronen, A.; Rinta, H.; Lahtinen, M. N···I Halogen Bonding Supported Stabilization of a Discrete Pseudo-Linear [I12]2− Polyiodide. *CrystEngComm* **2015**, *17*, 1736–1740. [CrossRef]
13. Alkorta, I.; Elguero, J.; Frontera, A. Not Only Hydrogen Bonds: Other Noncovalent Interactions. *Crystals* **2020**, *10*, 180. [CrossRef]

14. Van Megen, M.; Reiss, G.J. $I_6^{2-}$ Anion Composed of Two Asymmetric Triiodide Moieties: A Competition between Halogen and Hydrogen Bond. *Inorganics* **2013**, *1*, 3–13. [CrossRef]
15. Savastano, M.; Bazzicalupi, C.; García-Gallarín, C.; López de la Torre, M.D.; Pichierri, F.; Bianchi, A.; Melguizo, M. Anion Complexes with Tetrazine-Based Ligands: Formation of Strong Anion−π Interactions in Solution and in the Solid State. *Inorg. Chem.* **2016**, *55*, 8013–8024. [CrossRef]
16. Savastano, M.; García-Gallarín, C.; Giorgi, C.; Gratteri, P.; López de la Torre, M.D.; Bazzicalupi, C.; Bianchi, A.; Melguizo, M. Solid State and Solution Study on the Formation of Inorganic Anion Complexes with a Series of Tetrazine-Based Ligands. *Molecules* **2019**, *24*, 2247. [CrossRef] [PubMed]
17. Savastano, M.; Bazzicalupi, C.; García-Gallarín, C.; López de la Torre, M.D.; Bianchi, A.; Melguizo, M. Supramolecular forces and their interplay in stabilizing complexes of organic anions: Tuning binding selectivity in water. *Org. Chem. Front.* **2019**, *6*, 75–86. [CrossRef]
18. Savastano, M.; Bazzicalupi, C.; García-Gallarín, C.; Giorgi, C.; López de la Torre, M.D.; Pichierri, F.; Bianchi, A.; Melguizo, M. Halide and hydroxide anion binding in water. *Dalton Trans.* **2018**, *47*, 3329–3338. [CrossRef]
19. Savastano, M.; García-Gallarín, C.; López de la Torre, M.D.; Pichierri, F.; Bazzicalupi, C.; Bianchi, A.; Melguizo, M. Interplay between salt bridge, hydrogen bond and anion-π interactions in thiocyanate binding. *Inorg. Chim. Acta* **2018**, *470*, 133–138. [CrossRef]
20. Savastano, M.; Bazzicalupi, C.; Mariani, P.; Bianchi, A. Network Formation via Anion Coordination: Crystal Structures Based on the Interplay of Non-Covalent Interactions. *Molecules* **2018**, *23*, 572. [CrossRef]
21. Savastano, M.; Bazzicalupi, C.; García-Gallarín, C.; Gellini, C.; López de la Torre, M.D.; Mariani, P.; Pichierri, F.; Bianchi, A.; Melguizo, M. Iodide and triiodide anion complexes involving anion–π interactions with a tetrazine-based receptor. *Dalton Trans.* **2017**, *46*, 4518–4529. [CrossRef] [PubMed]
22. Savastano, M.; García-Gallarín, C.; López de la Torre, M.D.; Bazzicalupi, C.; Bianchi, A.; Melguizo, M. Anion-π and lone pair-π interactions with s-tetrazine-based ligands. *Coord. Chem. Rev.* **2019**, *397*, 112–137. [CrossRef]
23. Müller, M.; Albrecht, M.; Gossen, V.; Peters, T.; Hoffmann, A.; Raabe, G.; Valkonen, A.; Rissanen, K. Anion–π interactions in salts with polyhalide anions: Trapping of $I_4^{2-}$. *Chem. Eur. J.* **2010**, *16*, 12446–12453. [CrossRef] [PubMed]
24. Ilioudis, C.A.; Steed, J.W. Complexation of $I_4^{2-}$ and $I_8^{2-}$ by protonated azacyclophanes. *CrystEngComm* **2004**, *6*, 239–242. [CrossRef]
25. Savastano, M.; Martínez-Camarena, A.; Bazzicalupi, C.; Delgado-Pinar, E.; Llinares, J.M.; Mariani, P.; Verdejo, B.; García-España, E.; Bianchi, A. Stabilization of Supramolecular Networks of Polyiodides with Protonated Small Tetra-azacyclophanes. *Inorganics* **2019**, *7*, 48. [CrossRef]
26. Odell, B.; Reddington, M.V.; Slawin, A.M.Z.; Spencer, N.; Fraser Stoddart, J.; Williams, D.J. Cyclobis(paraquat-p-phenylene). A Tetracationic Multipurpose Receptor. *Angew. Chem. Int. Ed. Engl.* **1988**, *27*, 1547–1550. [CrossRef]
27. Savastano, M.; Bazzicalupi, C.; Bianchi, A. Porous Frameworks Based on Supramolecular Ball Joints: Bringing Flexibility to Ordered 3D Lattices. *Chem. Eur. J.* **2020**. [CrossRef]
28. Savastano, M.; Bazzicalupi, C.; Gellini, C.; Bianchi, A. Infinite supramolecular pseudo-polyrotaxane with poly[3]catenane axle: Assembling nanosized rings from mono- and diatomic $I^-$ and $I_2$ tectons. *Chem. Commun.* **2020**, *56*, 551–554. [CrossRef]
29. Krause, L.; Herbst-Irmer, R.; Sheldrick, G.M.; Stalke, D. Comparison of silver and molybdenum microfocus X-ray sources for single-crystal structure determination. *J. Appl. Cryst.* **2015**, *48*, 3–10. [CrossRef]
30. Sheldrick, G.M. SHELXT-Integrated space-group and crystal-structure determination. *Acta Cryst.* **2015**, *C71*, 3–8. [CrossRef]
31. Macrae, C.F.; Sovago, I.; Cottrell, S.J.; Galek, P.T.A.; McCabe, P.; Pidcock, E.; Platings, M.; Shields, G.P.; Stevens, J.S.; Towler, M.; et al. Mercury 4.0: From visualization to analysis, design and prediction. *J. Appl. Cryst.* **2020**, *53*, 226–235. [CrossRef] [PubMed]
32. Turner, M.J.; McKinnon, J.J.; Wolff, S.K.; Grimwood, D.J.; Spackman, P.R.; Jayatilaka, D.; Spackman, M.A. CrystalExplorer17. Available online: http://hirshfeldsurface.net (accessed on 8 May 2020).
33. Spackman, M.A.; Byrom, P.G. A novel definition of a molecule in a crystal. *Chem. Phys. Lett.* **1997**, *267*, 215–220. [CrossRef]
34. McKinnon, J.J.; Spackman, M.A.; Mitchell, A.S. Novel tools for visualizing and exploring intermol-ecular interactions in molecular crystals. *Acta Cryst. B* **2004**, *60*, 627–668. [CrossRef]

35. Spackman, M.A.; McKinnon, J.J. Fingerprinting intermolecular interactions in molecular crystals. *CrystEngComm* **2002**, *4*, 378–392. [CrossRef]
36. Which is correct under commonly employed and relatively diluted concentration ranges, but not an absolute truth.
37. Ramette, R.W.; Sandford, R.W., Jr. Thermodynamics of Iodine Solubility and Triiodide Ion Formation in Water and in Deuterium Oxide. *J. Am. Chem. Soc.* **1965**, *87*, 5001–5005. [CrossRef]